ACS APPLIED POLYMER MATERIALS

pubs.acs.org/acsapm Article

A Polysulfone/Cobalt Metal–Organic Framework Nanocomposite Membrane with Enhanced Water Permeability and Fouling Resistance

Eva Gil, Xiaochuan Huang, Kuichang Zuo, Jun Kim, Susana Rincón, José María Rivera, Kiarash Ranjbari, François Perreault, Pedro Alvarez, Alejandro Zepeda,* and Qilin Li*

Cite This: ACS Appl. Polym. Mater. 2022, 4, 3532–3542 Read Online

ACCESS | Metrics & More | Article Recommendations | Supporting Information

ABSTRACT: Ultrafiltration membranes are widely used in water and wastewater applications. The two most important membrane characteristics that determine the cost-effectiveness of an ultrafiltration membrane process are membrane permeability and fouling resistance. Metal–organic frameworks (MOFs) have been intensively investigated as highly selective sorbents and superior (photo) catalysts. Their potential as membrane modifiers has also received attention recently. In this study, a non-functionalized, water-stable, nanocrystalline mixed ligand octahedral MOF containing carboxylate and amine groups with a cobalt metal center (MOF-Co) was incorporated into polysulfone (PSF) ultrafiltration (UF) membranes at a very low nominal concentration (2 and 4 wt %) using the conventional phase inversion method. The resultant PSF/MOF-Co_4% membrane exhibited water permeability up to 360% higher than of the control PSF membrane without sacrificing the selectivity of the membrane, which had not been previously achieved by an unmodified MOF. In addition, the PSF/MOF-Co_4% membrane showed strong resistance to fouling by natural organic matter (NOM), with 87 and 83% reduction in reversible and irreversible NOM fouling, respectively, compared to the control PSF membrane. This improvement was attributed to the increases in membrane porosity and surface hydrophilicity resulting from the high hydrophilicity of the MOF-Co. The capability of increasing membrane water permeability and fouling resistance without compromising membrane selectivity makes the MOF-Co and potentially other hydrophilic MOFs excellent candidates as membrane additives.

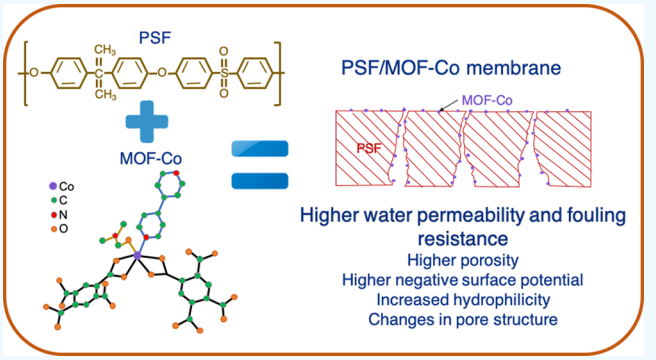

KEYWORDS: *metal–organic framework (MOF), nanocomposite membrane, membrane permeability, organic fouling, mixed matrix membranes (MMMs)*

1. INTRODUCTION

Membrane filtration has become a widely used water treatment method over the last three decades. It offers multiple advantages over conventional treatment methods, including superior treated water quality, compact modular configuration, automated operation, high water recovery, and low chemical consumption.[1,2] Key performance parameters of a water filtration membrane include water permeability, selectivity, and fouling resistance, which determine the water production rate, contaminant removal, long-term performance, and lifetime of the membrane. These performance parameters strongly depend on the porosity, pore structure, and surface properties of the membrane.[1,2] Therefore, a significant amount of research has been devoted to improving these membrane properties.

Chemical treatment to create hydrophilic functional groups on the membrane surface,[3] addition of modifiers (e.g., macromolecules[4] and nanoparticles of different size, morphology, and chemical composition[5−7]) into the polymer matrix, and surface coating[8] are three methods commonly utilized to enhance membrane performance. These modification methods have been shown to improve membrane permeability and reduce foulant attachment by increasing membrane hydrophilicity and catalyzing degradation of organic foulants and/or imparting antibacterial effects to hinder biological fouling.[5−8] For example, Celik et al.[6] showed that the addition of acid-treated multiwalled carbon nanotubes (MWCNTs) into a polyethersulfone (PES) membrane greatly increased membrane clean water flux and reduced natural organic matter

Received: January 22, 2022
Accepted: April 4, 2022
Published: April 20, 2022

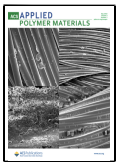

https://doi.org/10.1021/acsapm.2c00132
ACS Appl. Polym. Mater. 2022, 4, 3532−3542

(NOM) fouling by 63.1%. Zodrow et al.[7] incorporated silver nanoparticles into PSF UF membranes and demonstrated 99% reduction in bacterial growth and biofouling. Yu et al.[8] demonstrated that MnO_2 nanoparticles coated on the PVDF UF membrane catalyzed hydroxyl free radical formation by ozone decomposition and significantly reduced fouling by NOM, proteins, and polysaccharides. However, addition of membrane modifiers often leads to changes in the membrane structure. For example, the low compatibility between inorganic modifiers and the membrane polymer may lead to the formation of voids/defects at the modifier polymer interface[9] and/or changes in phase behavior.[10] These changes may compromise the membrane separation performance, e.g., reduction in contaminant rejection,[9] and therefore pose a major challenge in the fabrication of such mixed matrix membranes (MMMs).

Metal−organic frameworks (MOFs) are mesoporous materials formed by metal ions coordinated by organic linkers. MOFs of a wide variety of structures can be synthesized using diverse types of metal centers and organic linkers.[11] Their high porosity, diverse and tunable chemical composition, and, very importantly, high organic content and consequently excellent compatibility and affinity with common membrane polymers make MOFs highly attractive additives for MMMs. A few studies have shown the promise of MOF as a membrane modifier. Zhu et al.[12] prepared an aromatic poly(*m*-phenyleneisophthalamide) nanofiltration (NF) membrane containing MOF MIL-53(Al) by phase inversion and showed 78.2% higher water permeance. Low et al.[13] added a two-dimensional zeolitic imidazolate framework (ZIF-L) with leaf-shaped morphology into a PES membrane and reported a 75% increase in clean water flux and 29% decrease in transmembrane pressure increase caused by bovine serum albumin (BSA) fouling. The enhanced flux and BSA fouling resistance were attributed to increased membrane surface porosity, higher negative surface zeta potential, and reduced surface roughness. In another study, Sun et al.[14] showed the importance of MOF hydrophilicity in MMM performance: Tannic acid (TA)-modified hollow zeolitic imidazolate framework-8 (hZIF-8) greatly increased clean water flux (by up to 180%), BSA fouling resistance, and mechanical strength of a PSF membrane. Although the MOF modifiers had much less impact on the separation function of the membrane than inorganic modifiers, the MMMs reported in these studies showed increased pore size or molecular weight cutoff, suggesting loss in membrane selectivity. In another study, Prince et al.[15] incorporated Ag nanoparticle capped with polyethyleneimine anchored on poly(acrylonitrile-*co*-maleic acid) (PANCMA) into a PES membrane to enhance biofouling resistance. The modified membrane showed a clean water flux of 39.4% higher than that of the PES control membrane despite a slight decrease in pore size as a result of a higher polymer concentration used. The increase in flux was attributed to the hydrophilicity of the PANCMA. However, the separation function of the membrane was not characterized.

Many existing studies chose to functionalize MOFs post-synthesis to improve the hydrophilicity of the MOF and increase their compatibility with the membrane polymer. However, this adds complexity to the fabrication process. It is therefore highly desirable to evaluate MOFs that contain hydrophilic functional groups, such as amine, carboxyl, and hydroxyl groups in their organic linkers to understand their interactions with membrane polymers, impacts on the membrane formation process, and the resulting membrane characteristics as well as water permeability and separation functions. These MOFs can potentially achieve better membrane performance with a simpler synthesis process.

In this study, we report the fabrication of a mixed matrix UF membrane using a non-functionalized, water stable, nanocrystalline mixed ligand octahedral MOF containing carboxylate and amine groups with a cobalt metal center (MOF-Co). The impact of MOF-Co on basic membrane characteristics including porosity, surface hydrophilicity, roughness, and zeta potential as well as performance parameters including water permeability, solute rejection, and resistance to NOM fouling was thoroughly evaluated. Addition of a very small amount of MOF-Co (2 and 4 wt % in the membrane casting solution) was shown to drastically improve membrane permeability and fouling resistance without compromising membrane selectivity.

2. MATERIALS AND METHODS

2.1. Materials. Cobalt nitrate hexahydrate ($Co(NO_3)_2{\cdot}6H_2O$, 98.0%), 4,4′-bipyridine (98.0%), 1,2,4,5-benzenetetracarboxylic acid (H_4BTEC, 96%), *N*,*N*-dimethylformamide (DMF, 99.8%), poly(vinyl pyrrolidone) (PVP, MW: 55,000), *N*-methyl-2-pyrrolidone (NMP, 99.5%), sodium dodecyl sulfate (SDS, 98.5%), polysulfone (PSF, MW 22,000), and polyethylene glycol (PEG, with MW of 10, 35, 100, 200, and 400 kDa) were purchased from Sigma-Aldrich Co. Sodium hydroxide standard (NaOH, 1 N), hydrochloric acid standard (HCl, 1 N), and calcium chloride ($CaCl_2$, 96.0%) were purchased from Thermo Fisher Scientific. Sodium chloride (NaCl) was purchased from EMD Millipore. Suwannee River aquatic NOM was purchased from International Humic Substances Society, St. Paul, MN.

2.2. Synthesis and Characterization of MOF-Co. The pillared layer MOF Co_2(btec)(bipy)$(DMF)_2$ ($C_{26}H_{24}Co_2N_4O_{10}$, referred to as MOF-Co) was synthesized using a simple solvothermal method previously reported.[16] Briefly, 0.094 g of 4,4′-bipyridine, 0.153 g of H_4BTEC, 0.35 g of $Co(NO_3)_2{\cdot}6H_2O$, and 15 mL of DMF were mixed in a crystal reactor and reacted at 90 °C for 68 h. The solution was then heated in an oven at 105 °C for 0.5 h to complete the synthesis. The product was washed with chloroform and dried at 105 °C for 24 h. The chemical composition of MOF-Co was characterized by attenuated total reflectance-Fourier transform infrared spectroscopy (ATR-FTIR) (Varian, model 640 IR) in the 4000−500 cm^{-1} wavenumber range, X-ray powder diffraction (XRD) using a Bruker D-8 Advance diffractometer at 1 s and a step size of 0.02°, and thermal gravimetric analysis-differential thermogravimetry (TGA-DTG) (Discovery TGA series, TA Instruments) at a heating rate of 10 °C/min in the range of 30−700 °C in a nitrogen environment. The morphology of MOF-Co was examined using field emission scanning electron microscopy (FESEM) (Joel model 7600F). The particle size was measured using a Zetasizer Nano ZS (Malvern) by dispersing MOF-Co particles in DI water (pH = 6.4). Finally, the pore dimeter, total pore volume, and surface area of MOF-Co were characterized using a Brunauer−Emmett−Teller (BET) analyzer (Autosorb-iQ-MP/Kr, Quantachrome Instruments, USA). During the BET test, the MOF-Co samples were first degassed at 140 °C for 24 h and then analyzed in a liquid nitrogen bath at a temperature of −195.8 °C.

2.3. Membrane Fabrication. PSF ultrafiltration membranes were made using the wet phase inversion process. First, 8 wt % of PVP was dissolved in NMP with stirring. For preparation of the PSF/MOF-Co membranes, different amounts of MOF-Co (0.025, 0.625, 1.0, 2.0, or 4.0 wt % in the final casting solution) were dispersed in the PVP solution using an ultrasonication probe (Sonics Materials VCX 500 Ultrasonic Microprocessor) for 15 min at 40% power. At 2 and 4 wt %, MOF-Co dispersed well in the PVP solution and led to notable changes in the membrane structure and performance as discussed later. Therefore, the results were only reported for these two MOF-Co concentrations hereafter. Then, PSF was added to reach a final concentration of 15 wt % in the casting solution. The solution was

https://doi.org/10.1021/acsapm.2c00132
ACS Appl. Polym. Mater. 2022, 4, 3532−3542

stirred overnight to ensure complete dissolution of PSF. The cast solution was allowed to set until all air bubbles disappeared and sonicated again using the ultrasonication probe for 15 min at 40% power. To fabricate the membranes, the casting solution was deposited onto a glass plate using an aluminum casting knife with a thickness setting of 250 μm (Gardco, USA), quickly transferred to a 60 °C water bath, and kept submerged for 20 min. The membrane formed was then removed from the water bath, rinsed thoroughly, and stored in fresh deionized water for later use. Table 1 shows the compositions of casting solutions for the membranes studied. The PSF/MOF-Co membranes prepared with 2 and 4 wt % of MOF-Co in the casting solution were denoted as PSF/MOF-Co_2% and PSF/MOF-Co_4%, respectively.

Table 1. Composition of Casting Solution

membrane	PSF (wt %)	PVP (wt %)	NMP (wt %)	MOF-Co (wt %)
PSF	15.0	8.0	77.0	0.0
PSF/MOF-Co_2%	15.0	8.0	75.0	2.0
PSF/MOF-Co_4%	15.0	8.0	73.0	4.0

2.4. Membrane Characterization. Membrane samples were characterized for surface and cross-sectional morphology and elemental composition by scanning electron microscopy (SEM, FEI Quanta 400 FEG, 20 kV) with a TEAM Software Suite, coupled with Octane Elect and Octane Elite energy-dispersive spectroscopy (EDS). For cross-sectional images, dry membrane samples were treated in liquid nitrogen and fractured to retain the membrane pore structure. All samples were sputter-coated with a 10 nm layer of gold in vacuum before SEM analysis (CrC-150 Sputtering TORR International).[7]

The three-dimensional surface morphology and roughness of the membranes were characterized by atomic force microscopy (AFM, Park AFM NX20 Microscope). Samples with an effective area of around 0.5 cm^2 were mounted on sample holders using a carbon tape and scanned in tapping mode (scan size of 1 μm × 1 μm, scan rate of 1 Hz) using a silicon AFM probe (TESPA-V2, Bruker, USA). The arithmetic mean roughness (R_a) was calculated using the Park SmartScan Operating Software (Bruker, USA).[13]

The overall porosity (ε) of the membranes was determined via the gravimetric method. Membrane samples were immersed in deionized water for 48 h to saturate all membrane pores with water. The weights of the wet membranes were measured after removing the excessive water on the membrane surface using tissue paper. The membranes were then dried in an oven at 50 °C for 24 h, and the weight of the dry membranes was measured.[17] The membrane porosity was then calculated using the following equation (eq 1):[18]

$$\varepsilon = \frac{W_w - W_d}{d_w \times A \times l} \quad (1)$$

where W_w and W_d are the weights (g) of the wet and dry membranes, respectively, A (cm^2) is the membrane area, d_w (0.998 g/cm^3) is the density of water, and l (cm) is the membrane thickness determined from the cross-sectional SEM images.

Membrane surface potential and hydrophilicity were characterized to determine the impact of MOF-Co on surface properties of the membrane. Membrane surface zeta potential was determined by streaming potential measurements using a ZetaCAD analyzer with a flat surface sample cell (CAD Instrumentation; Les Essarts Le Roi, France). Sample coupons of 2.5 cm × 7.5 cm were placed in a clamping cell, and measurements were performed in an electrolyte solution containing 1 mM KCl and 0.1 mM $KHCO_3$. The pH of the electrolyte solution was adjusted to 11, 10, 9, 8, 7, 6, 5, and 4 using KOH or HCl for each measurement.[19] Membrane surface hydrophilicity was characterized by water contact angle measurements using a drop shape analyzer (DSA100).

2.5. Membrane Permeability and Separation Property. The water permeability of the membranes was determined by filtration experiments using deionized water as the feed. The schematic diagram of the filtration experimental setup is shown in Figure S1 in the Supporting Information. A 200 mL continuously stirred filtration cell (Amicon 8200, USA) houses a membrane of 6.4 cm in diameter with an effective membrane area of 28.7 cm^2. The filtration cell is connected to a stainless-steel feed reservoir pressurized by a nitrogen tank. Permeate is collected in a glass container placed on a digital balance (Ohaus, Adventure Pro Precision Balance, model AV8101) interfaced with a laptop to determine permeate flux. The cumulative mass of the permeate was recorded every 60 s, and the water flux was determined by linear regression of the permeate mass versus time curve.[20]

Filtration was carried out at applied pressures ranging from 1 to 3 bar at room temperature. The applied pressure was first established at 1 bar and successively increased to 3 bar with 0.5 bar increments. At each transmembrane pressure, water flux was recorded for at least 20 min after a stable water flux was established. Then, the applied pressure was successively decreased from 3 down to 1 bar with 0.5 bar increments, and water flux was measured at each applied pressure. The membrane water permeability L_p (L/m^2-h-bar) is defined in eq 2, where J_w (L/m^2-h) and ΔP (bar) are the clean water flux and applied pressure, respectively.[21] L_p was determined by linear regression of the J_w versus ΔP curve.

$$L_p = \frac{J_w}{\Delta P} \quad (2)$$

The membranes' separation properties were characterized by determining rejection of PEG of different molecular weights, i.e., 10, 35, 100, 200, and 400 kDa. Filtration was performed using a 50 mg/L PEG solution at an initial flux of 100 L/m^2-h (LMH) for each PEG. After each filtration, the membrane was thoroughly cleaned with SDS and DI water to remove all residue. PEG concentrations in the feed and permeate solutions were measured using a high sensitivity total organic carbon (TOC) analyzer (TOC-LCSH/CSN with auto-sampler ASI-L, Shimadzu, Japan). The rejection of PEG (R) by different membranes was calculated using the following equation (eq 3):[12]

$$R = \left(1 - \frac{C_p}{C_f}\right) \times 100 \quad (3)$$

where C_p and C_f are the PEG concentrations in the permeate and the feed solutions, respectively.

2.6. Membrane Fouling Resistance. *2.6.1. Model Foulant.* The fouling behaviors of the control and PSF/MOF-Co membranes were assessed using Suwannee River aquatic NOM (1R101N, International Humic Substances Society, St. Paul, MN) as the model organic foulant. The Suwannee River aquatic NOM consists of 8.5% H_2O, 52.47% C, 4.19% H, 42.69% O, 1.1% N, 0.65% S, 0.02% P, and 7% (p/p) inorganic residue. It contains a large number of chemical functional groups including carboxyls (9.85 meq/g) and phenolics (3.94 meq/g C). NOM is the primary organic foulant in drinking water sources as well as wastewater. NOM stock solution (1 g/L) was prepared by adding the as-received aquatic NOM powder into deionized water, adjusting the pH to 8 with 1 N NaOH, and stirring overnight to ensure complete dissolution. The solution was filtered through a 0.45 μm nylon membrane and stored in a sterilized amber glass bottle at 4 °C until use.[22]

All fouling experiments were conducted using a feed solution containing 20 mg/L NOM, 7 mM NaCl, and 1 mM $CaCl_2$ (a total ionic strength of 10 mM). The NOM concentration was confirmed by measuring the TOC of the feed solution using a high sensitivity TOC analyzer. The measured TOC concentration was consistent with that calculated from the mass concentration of the aquatic NOM and its organic carbon content provided by the International Humic Substances Society.[22]

2.6.2. Membrane Fouling Experiments. Fouling experiments were performed in the filtration system, as shown in Figure S1. All

https://doi.org/10.1021/acsapm.2c00132
ACS Appl. Polym. Mater. 2022, 4, 3532−3542

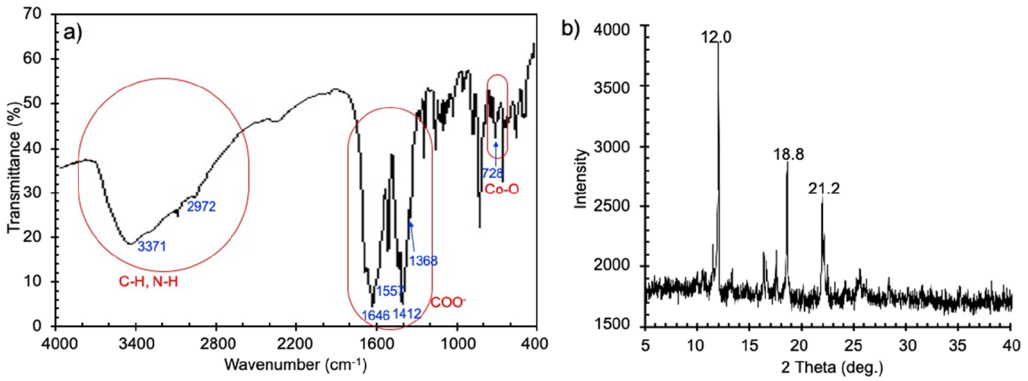

Figure 1. FTIR (a) and XRD (b) spectra of the MOF-Co.

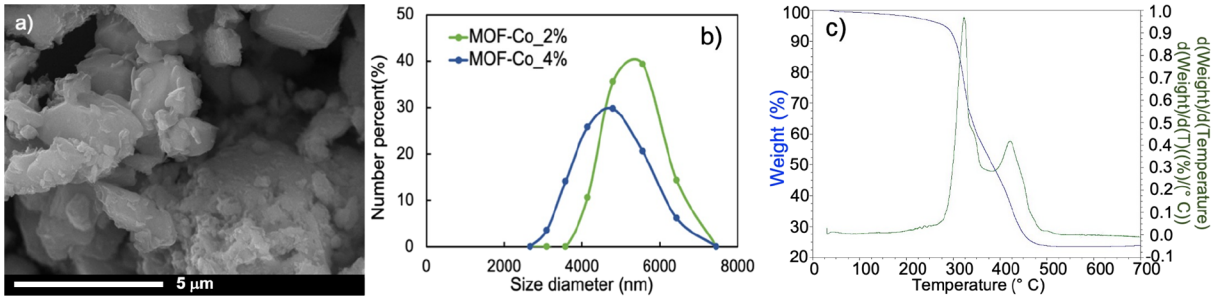

Figure 2. (a) FESEM image of MOF-Co, (b) particle size of MOF-Co dispersed in DI water, and (c) TGA and DTG curves of the MOF-Co.

experiments were carried out at room temperature (22 °C) in duplicates. The experimental protocol consisted of three steps: compaction, fouling, and cleaning. The membrane was first compacted by filtering deionized water at an applied pressure of 3 bar until the permeate flux stabilized. Next, the pressure was lowered to reach a desired initial clean water flux of 108 L/m^2-h (J_{BF}), which was kept constant in all fouling experiments.[23] After compaction, the stirred cell was fed with the NOM feed solution. The filtration was carried out at the same pressure for 2 h, and the magnetic stirrer in the cell was controlled at 225 rpm to provide a hydraulic shear on the membrane surface. At the end of the fouling step, the pressure was released, and the fouled membrane was hydraulically washed using DI water by magnetic stirring at 1000 rpm for 10 min and rinsed thoroughly with DI water. Filtration was then resumed with DI water at the same applied pressure, and the permeate flux was measured again (J_{AF}).

Fouling behavior of the membranes was characterized by the overall hydraulic resistance of the fouling layer formed during the fouling stage of the filtration experiment as well as the resistance caused by irreversible fouling, defined as the remaining fouling layer resistance after DI water cleaning. Determination of these quantitative fouling indices is described below.

During filtration of the NOM feed solution, the total hydraulic resistance (R_t) of a fouled membrane is the sum of the intrinsic membrane resistance R_m and the resistance of the reversible (R_r) and irreversible (R_{ir}) fouling layer (eq 4) and can be determined from the membrane flux at the end of the fouling stage J_F (eq 5):

$$R_t = R_m + R_{ir} + R_r \tag{4}$$

$$R_t = \frac{TMP}{\mu \times J_F} \tag{5}$$

Here, TMP is the transmembrane pressure (Pa) and μ is the water viscosity (Pa·s). R_m can be determined from the baseline clean water flux J_{BF}, i.e., flux before fouling, for each specific membrane sample

$$R_m = \frac{TMP}{\mu \times J_{BF}} \tag{6}$$

After DI water cleaning, the reversible fouling layer was removed. Therefore, the difference in total hydraulic resistance before and after DI water cleaning is considered the reversible fouling resistance R_r (eq 7):

$$R_r = \frac{TMP}{\mu \times J_F} - \frac{TMP}{\mu \times J_{AF}} \tag{7}$$

Here, J_F is the membrane flux at the end of the fouling stage and J_{AF} is the clean water flux after DI water cleaning.

The remaining hydraulic resistance after cleaning consists of R_m and R_{ir}. Irreversible fouling layer resistance R_{ir} can then be calculated from the difference between the hydraulic resistance after cleaning and R_m

$$R_{ir} = \frac{TMP}{\mu \times J_{AF}} - R_m \tag{8}$$

Flux recovery (FR) after cleaning is another quantitative measure of the reversible versus irreversible fouling resistance of a membrane. It is defined as the ratio between the clean water flux of the membrane after fouling and cleaning and the clean water flux of the fresh membrane (eq 9)[13]

$$FR = \frac{J_{AF}}{J_{BF}} \times 100\% \tag{9}$$

3. RESULTS AND DISCUSSION

3.1. Synthesis and Characterization of MOF-Co. The MOF-Co synthesized was characterized by ATR-FTIR, XRD, FESEM, TGA, and BET. The FTIR spectrum of the MOF-Co (Figure 1a) shows characteristic peaks of C−H and N−H stretching at 2972 and 3371 cm^{-1}, respectively, as well as those of carboxylate functional groups at 1557−1646 and 1368−1412 cm^{-1}. The Co−O peak at 728 cm^{-1} confirms the presence of Co(BTEC).[24] These results are consistent with the functional groups expected in the MOF-Co.[16] Moreover, the

https://doi.org/10.1021/acsapm.2c00132
ACS Appl. Polym. Mater. 2022, 4, 3532−3542

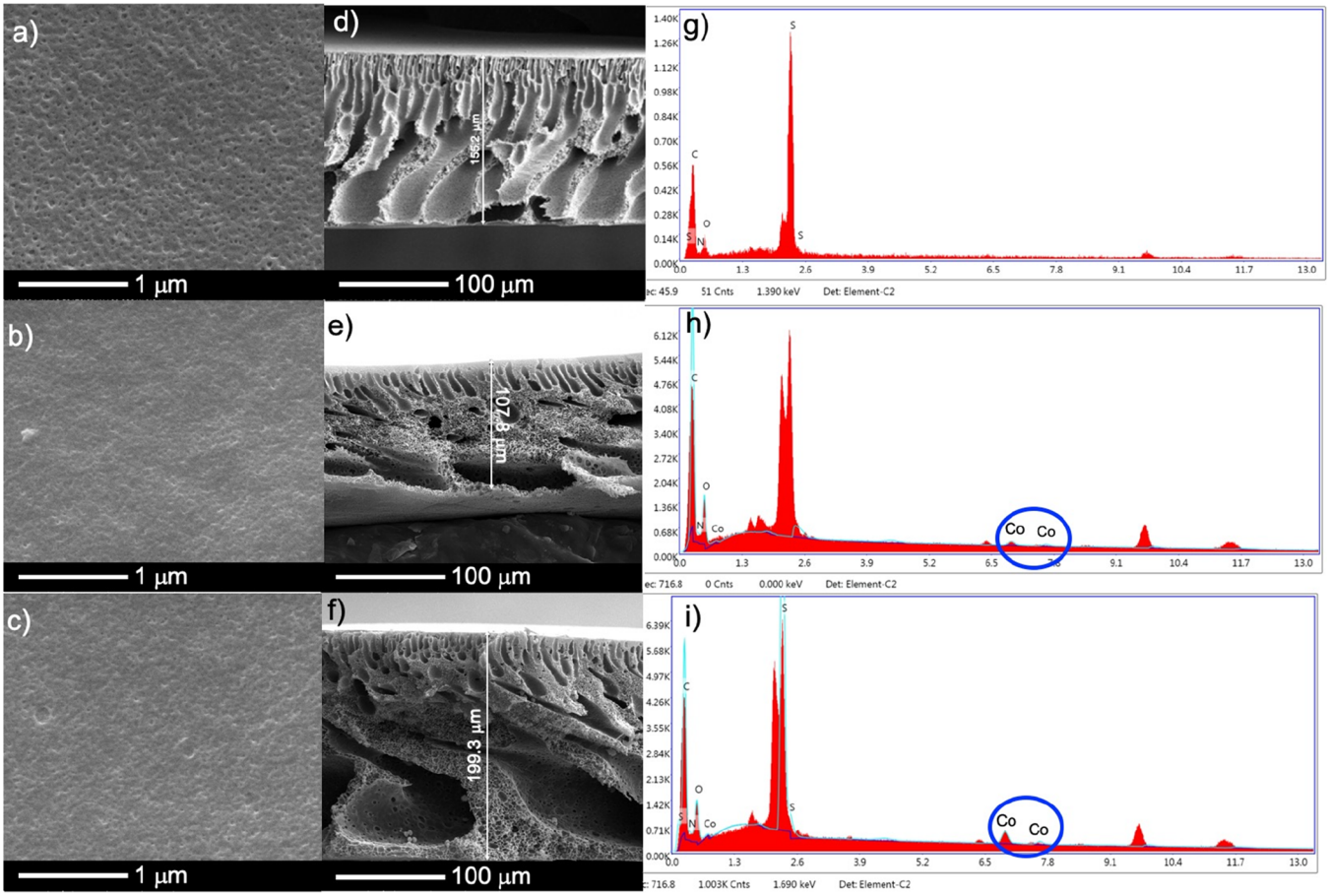

Figure 3. Surface SEM images of (a) PSF, (b) PSF/MOF-Co_2%, and (c) PSF/MOF-Co_4% membranes. Cross-sectional SEM images of (d) PSF, (e) PSF/MOF-Co_2%, and (f) PSF/MOF-Co_4% membranes. The EDS spectra of (g) PSF, (h) PSF/MOF-Co_2%, and (i) PSF/MOF-Co_4% membranes.

XRD pattern shows characteristic peaks at 2θ angles of 12, 18.8, and 21.2° (Figure 1b). All these signals confirm that the material has the same structure as that previously reported by Song et al.[16]

The FESEM image (Figure 2a) of MOF-Co shows a wide range of MOF-Co crystal sizes. Dynamic light scattering analysis using the Zetasizer Nano shows that the average particle size of MOF-Co dispersed in water is 1279 ± 60.8 nm in diameter (Figure 2b). The TGA-DTG spectrum in Figure 2c suggests that the MOF-Co is stable at a temperature <300 °C, above which the material starts to collapse. The strongly coordinated DMF molecules in the MOF-Co structure were removed when the MOF framework collapsed, which occurred at 322.3 °C. N_2 adsorption/desorption analyses show that the dry MOF-Co has a specific surface area of 353.39 m^2/g and an average pore width of 2.89 nm.[25]

3.2. Membrane Characterization of PSF and PSF/MOF-Co. *3.2.1. Membrane Morphology.* SEM images of the PSF and PSF/MOF-Co membranes are shown in Figure 3. As shown in Figure 3a, the surface pore size of the PSF membrane was mostly less than 50 nm, which is in line with that of a UF membrane. The cross-sectional SEM image (Figure 3d) shows the typical structure of asymmetric UF membranes prepared by the wet phase inversion method: a thin, dense, active layer supported by a macroporous sublayer with finger-like pores and macro voids. Membrane thickness was determined using the cross-sectional SEM images. At least three samples of each membrane type were characterized, and the measured thickness was averaged. The thicknesses of the membranes were 166.7 ± 10.3, 166.7 ± 36.1, and 187.6 ± 11.6 μm for PSF, PSF/MOF-Co_2%, and PSF/MOF-Co_4%, respectively. The addition of MOF-Co significantly changed the membrane pore structure. As shown in Figure 3b,c, the surface pore size of PSF/MOF-Co was notably smaller than that of the pristine PSF membrane. The number of finger-like pores in the transition zone from the finger-like pores to the macro voids was notably smaller (Figure 3e,f). Instead, the transition zone exhibited a sponge-like structure, with a large number of micrometer-sized pores. Furthermore, the size of the macro voids was much larger in the PSF/MOF-Co membranes. These changes may be attributed to the faster exchange of the solvent (NMP) and the non-solvent (water) in the phase inversion process as a result of the enhanced diffusion of water (non-solvent) in the presence of highly hydrophilic MOF-Co.[17,18,26] The presence of MOF-Co in the membrane matrix was confirmed by EDS and EDS mapping. The EDS spectra of PSF/MOF-Co_2% and PSF/MOF-Co_4% clearly show the presence of cobalt (Figure 3h,i). In addition, Co elemental mapping (Figure 4) shows that MOF-Co was well distributed throughout the PSF/MOF-Co_2% and PSF/MOF-Co_4% membranes, with higher density in the transition zone, where a sponge-like structure was dominant. A higher MOF-Co concentration in the casting solution resulted in higher MOF-Co content in the membranes produced. The MOF-

https://doi.org/10.1021/acsapm.2c00132
ACS Appl. Polym. Mater. 2022, 4, 3532−3542

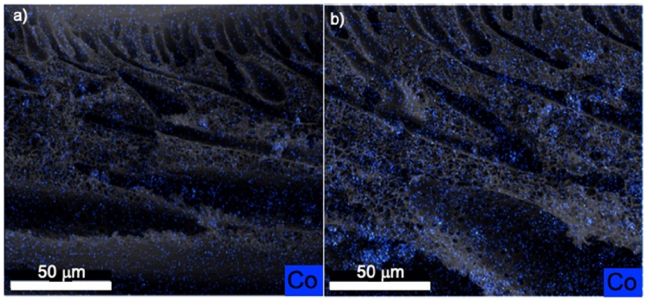

Figure 4. EDS mapping of Co on the cross section of (a) PSF/MOF-Co_2% and (b) PSF/MOF-Co_4% membranes.

Co contents of the dry membranes were estimated to be 3.3 and 7.0% for the PSF/MOF-Co_2% and PSF/MOF-Co_4% membranes, respectively, based on the S and Co contents of the membranes (Figure 3h,i).

3.2.2. Membrane Porosity. Figure 5 compares the overall porosity of the membranes measured using the gravimetric

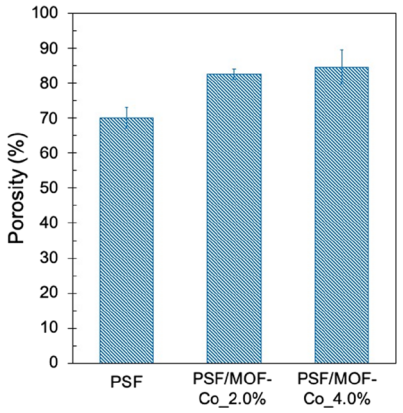

Figure 5. Membrane porosity before and after MOF-Co addition.

method. The addition of MOF-Co at 2 and 4 wt % in the casting solution increased the membrane porosity from 70.1 to 82.6 and 84.6%, a 12.5 and 14.5% increase, respectively. This is consistent with the pore structure change observed in the SEM images (Figure 3). As discussed above, the increase in porosity may be attributed to the increased formation of the polymer poor phase induced by the hydrophilic MOF-Co during the phase inversion process,[13] which increases the diffusion of the non-solvent (i.e., water) and therefore the pore size and overall membrane porosity. Similar effects have been reported for other hydrophilic modifiers.[5,17,26,27] The higher porosity is expected to increase membrane permeability, which is discussed later.

3.2.3. Membrane Surface Properties. AFM surface images and the corresponding arithmetic mean roughness R_a of all membranes are presented in Figure 6. All membrane surfaces were very smooth, with R_a values of 2.7 ± 0.4, 5.7 ± 0.5, and 2.6 ± 0.6 nm for the PSF, PSF/MOF-Co_2%, and PSF/MOF-Co_4%, respectively. The low R_a values together with the EDS mapping results (Figure 4) suggest that MOF-Co was well dispersed throughout the PSF matrix. The PSF/MOF-Co_2% appears to have more roughness than the PSF and the PSF/MOF-Co_4%. This is attributed to the faster exchange rate between NMP and water during the coagulation process due to the hydrophilicity of the MOF-Co. The presence of the MOF-Co in the active layer may also have contributed to the increased R_a in PSF/MOF-Co_2%.[14] The PSF/MOF-Co_4% surface had a similar R_a value as the PSF control membrane, but the surface features appear to be significantly smaller in the x and y dimensions, suggesting changes in polymer chain interactions due to the presence of MOF-Co in the active layer.

Figure 7a shows the surface zeta potential of the membranes as a function of pH. The addition of MOF-Co significantly

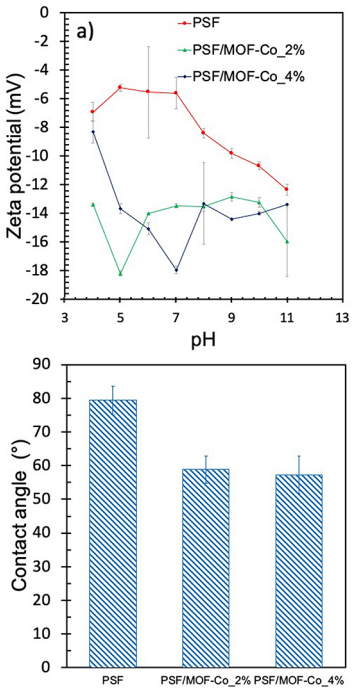

Figure 7. Zeta potential (a) and water contact angle (b) of the membranes before and after MOF-Co addition.

lowered membrane surface zeta potential. At pH 8, the membrane surface zeta potential decreased from −8.4 ± 0.32 mV for the PSF membrane to −13.54 ± 0.31 and −13.29 ± 2.8 for PSF/MOF-Co_2% and PSF/MOF-Co_4%, respectively. The more negative zeta potential further supports that

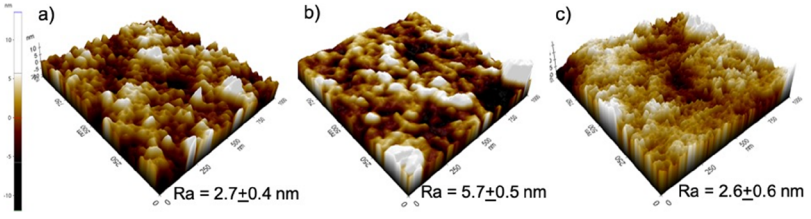

Figure 6. Roughness surface of the membranes: (a) PSF, (b) PSF/MOF-Co_2%, and (c) PSF/MOF-Co_4%.

https://doi.org/10.1021/acsapm.2c00132
ACS Appl. Polym. Mater. 2022, 4, 3532−3542

Table 2. Comparison of Reported MMM Performance

MMM with MOF	permeability change (%)	selectivity: target compound/ molecular weight	selectivity: rejection change (%)[a]	MOF content in the casting solution (%)	decrease in contact angle (%)[b]	reference
PSf/hZIF-8	184.28	BSA/66.38 kDa	0.7	2	11	14
UiO-66@GO/PES	337.01	methyl range (MO)/327.3 Da	5.28	3	16	30
MIL-53/PVDF	484.21	NA	NA	67	25	28
UiO-66-PSBMA/ PSf	150.83	BSA/66.38 kDa	−0.6	0.3	14	31
MOF-C300/PAN	60.01	mextran/NA	−1.17	1	NA	32
Co100-MOF-74/ PES	18.77	BSA/66.38 kDa	30.1	0.4	8	33
CA/MOF@$GO_{0.12}$	85.38	BSA/66.38 kDa	1.59	0.45	32	29
ZGO-NH/PES	64.52	BSA/66.38 kDa	0.13	1	19	34
UiO-66-NH 2 @ CQDs	182	BSA/66.38 kDa		0.5		35
PSF/MOF-Co_2%	255	PEG/10, 35, 100, 200, 400 kDa	[c]	2	26	this study
PSF/MOF-Co_4%	360	PEG/10, 35, 100, 200, 400 kDa	[c]	4	28	

[a]Rejection change = rejection of MMM − rejection of the control membrane. [b]Decrease in contact angle $= \frac{\text{contact angle of the control membrane} - \text{contact angle of MMM}}{\text{contact angle of the control membrane}} \times 100$. [c]No statistically significant difference from the control. NA: not available.

MOF-Co is present in the active layer, whose net negative charge led to the decrease in zeta potential.

The static water contact angle on the membrane surface was used to measure membrane surface hydrophilicity. The reported contact angle values were the average of at least five measurements each on four samples of the same membrane. The water contact angle on the membrane surface decreased from 79.4 ± 4.3 to 58.9 ± 4.0 and 57.2 ± 5.6° with 2 and 4% MOF-Co, respectively (Figure 7b), suggesting a significant decrease in membrane surface hydrophobicity due to the hydrophilic nature of MOF-Co that originated from the carboxylate and amine groups around the Co centers.[15,18] These changes in contact angle were among the highest in MOF-modified membranes reported so far (Table 2), presumably due to the higher hydrophilicity of the MOF-Co.[17]

3.3. Membrane Performance. *3.3.1. Water Flux.* Figure 8 shows the clean water flux as a function of applied pressure for the three membranes. The addition of MOF-Co into the PSF membrane greatly improved the water permeability of the membrane: from 114.01 L/m^2-h-bar for the control PSF membrane to 404.56 and 524.14 L/m^2-h-bar for PSF/MOF-Co_2% and PSF/MOF-Co_4% membranes, an increase of 255 and 360%, respectively. The permeability improvements are among the highest in composite UF membranes that have been reported (Table 2) and achieved with a relatively low dosage of MOF-Co (2 and 4% in the casting solution, 3.3 and 7% in the dry membrane). It is important to note that the majority of the MOFs used in the studies shown in Table 2 were functionalized to improve binding between the MOFs and the polymer matrix and hence enhance the permeability of the composite membrane. The process of MOF functionalization makes the synthesis process lengthier and more complex, which ultimately results in higher cost. The MIL-53(Fe), the only unfunctionalized MOF used in previous studies of Ren et al.,[28] was reported to improve the water flux by 484.2%. However, a very high MIL-53(Fe) loading, 67%, was required in the membrane casting solution, more than an order of magnitude higher than the MOF-Co content used in this study. The application of the as-synthesized MOF-Co in our study took advantage of the unique properties of MOF-Co, especially its hydrophilicity evidenced by the large decrease in contact angle in comparison with other membranes, as shown in Table 2; also, its mixed organic ligands have higher compatibility with the polymeric matrix of the membrane, resulting in greatly improved water permeability without sacrificing its selectivity in comparison with other MMMs, as shown in Table 2.

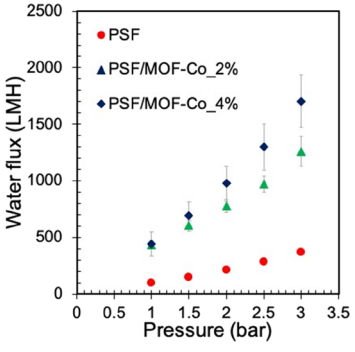

Figure 8. Water flux vs applied pressure. The flux was measured with both ascending and descending pressure ramps.

Even though the MOF-Co has a relatively low specific surface area, its high hydrophilicity led to more improvements in the performance of membranes than many other high specific surface area MOFs. Results from a limited number of previous studies also suggest an important role of MOF hydrophilicity. For example, Sun et al.[14] reported that tannic acid-modified ZIF-8 (hZIP-8) improved PSF membrane water permeability more than the unfunctionalized ZIF-8, even though its specific surface area (957 m^2/g) was significantly lower than the unfunctionalized ZIF-8 (1368 m^2/g). The better membrane performance was attributed to the hydrophilic surface of hZIF-8. Another study showed that the

https://doi.org/10.1021/acsapm.2c00132
ACS Appl. Polym. Mater. 2022, 4, 3532−3542

hydrophilic functional groups in a Ce-based MOF improved the hydrophilicity and consequently the water permeability of a PES membrane,[18] despite its low specific surface area (218.6 m^2/g).

Although the intrinsic pore structure of MOF-Co can provide additional paths for water transport,[14] the low porosity of the MOF-Co and the small amount added could not account for the large increase in membrane permeability. Such an extraordinary increase in membrane permeability is attributed to the higher membrane overall porosity, increased hydrophilicity, and changes in the membrane structure. As discussed previously, a hydrophilic additive in the membrane casting solution can lead to a more porous structure.[13] Furthermore, the increased membrane hydrophilicity, especially more hydrophilic pore walls and active layer surface, facilitates water transport through the membrane polymer.[29] It is important to note that significant changes in all these properties of the membrane occurred with a very low concentration of MOF-Co, suggesting excellent dispersion of MOF-Co in the polymer matrix as corroborated by the EDS mapping data (Figure 4). It is hypothesized that the small amount of MOF-Co preferentially accumulated at the polymer-water interface during the phase inversion process due to its excellent hydrophilicity. Therefore, MOF-Co was present primarily on the membrane pore wall and the active layer surface, leading to a large increase in membrane water permeability.

3.3.2. Molecular Weight Cutoff (MWCO). Conventional membrane materials suffer from the permeability-selectivity paradox, i.e., selectivity decreases with increasing permeability. Therefore, it is important to characterize both performance parameters. In this study, the selectivity of the membranes was characterized by rejection of PEG molecules of a wide range of molecular weights. Figure 9 shows the rejection of PEG as a function of PEG MW. Student's *t* test showed no statistically significant difference in PEG rejection between the PSF and the PSF/MOF-Co membranes, indicating that MOF-Co addition up to 4 wt % in the casting solution did not compromise membrane selectivity.

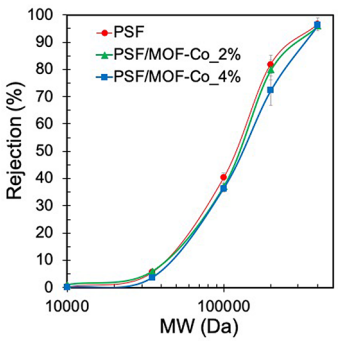

Figure 9. Rejection of PEG of different molecular weights by PSF and PSF/MOF-Co membranes. Data curves are added to aid the eyes only.

3.3.3. Fouling Resistance. Fouling behavior of the membranes was investigated using aquatic NOM as the model foulant. Feed water containing 20 mg/L NOM was filtered under constant pressure. Figure 10a compares the flux of the control PSF and PSF/MOF-Co membranes during the 2 h NOM fouling step. All membranes showed a notable flux decrease during the filtration of the NOM solution. Nevertheless, the PSF/MOF-Co membranes showed a significantly lower flux decrease, with normalized flux J/J_0 of 0.69 and 0.71 for PSF/MOF-Co_2% and PSF/MOF-Co_4%, respectively, compared to 0.56 for the PSF membrane at the end of the NOM filtration step.

Analyses of the fouling layer resistance show large reduction in both reversible and irreversible fouling layer resistances (Figure 10b) calculated using eqs 4−9. The reversible (R_r) and irreversible (R_{ir}) NOM fouling layer resistances on the PSF/MOF-Co_4% membrane were 87 and 83% lower than those of the control PSF membrane, respectively. Because the initial flux was kept the same in all fouling experiments, i.e., the same NOM mass transfer rate to the membrane surface, the lower R_r and R_{ir} suggest reduced deposition/attachment of NOM on the PSF/MOF-Co membrane surface and pore walls. This is attributed to the higher negative surface zeta potential, which increases electrostatic repulsion between the membrane and the negatively charged NOM molecules, and the increased hydrophilicity of the membrane, which reduces the hydrophobic interaction between NOM molecules and the membrane surface or pore walls.[36] These results are also consistent with the flux recovery (FR) measured after DI water cleaning (Figure 10c). The MOF-Co/PSF membranes achieved notably higher FR, up to 83%. In comparison, Feng et al.[35] prepared a PES membrane modified with a carbon quantum dot-modified MOF (UiO-66-NH_2@CQDs) and reached 77.6% FR after NOM fouling. On the other hand, the PSF/MOF-Co_4% showed slightly better fouling resistance than the PSF/MOF-Co_2% despite the similar surface zeta potential, hydrophilicity, and porosity. This may be attributed to the higher zeta potential (Figure 7a) and hydrophilicity of the pore wall, which cannot be measured by the streaming potential and contact angle measurement method used.

4. CONCLUSIONS

In this study, we demonstrated the fabrication of a high-performance mixed matrix UF membrane by adding a small amount of a highly hydrophilic, water-stable, cobalt-based nanocrystalline MOF, MOF-Co, into the casting solution. The addition of MOF-Co led to a series of changes in membrane characteristics, including higher porosity, higher negative surface zeta potential, greater hydrophilicity, and notable changes in the pore shape/structure. As a result, MOF-Co-modified membranes exhibited greatly increased water permeability, up to 360% higher than the control PSF membrane, while maintaining the selectivity of the membrane. Furthermore, the MOF-Co-modified membranes greatly reduced both reversible and irreversible fouling by NOM, an ubiquitous organic foulant in water and wastewater. Compared with MOF materials used in previous studies, the MOF-Co amendment achieved extraordinary improvement in membrane performance with a low MOF-Co concentration. We attribute the excellent performance of the MOF-Co as a membrane modifier to its high intrinsic hydrophilicity due to the oxygen and nitrogen containing functional groups, which allows it to accumulate at the polymer-water interface during the phase inversion process and hence increases the hydrophilicity of the membrane pore wall and active layer surface. These findings show great potential of hydrophilic MOFs as a membrane modifier and underscore the importance of further investigation on the MOF-water-organic solvent interactions and their impacts on the membrane structure. In addition, the

https://doi.org/10.1021/acsapm.2c00132
ACS Appl. Polym. Mater. 2022, 4, 3532−3542

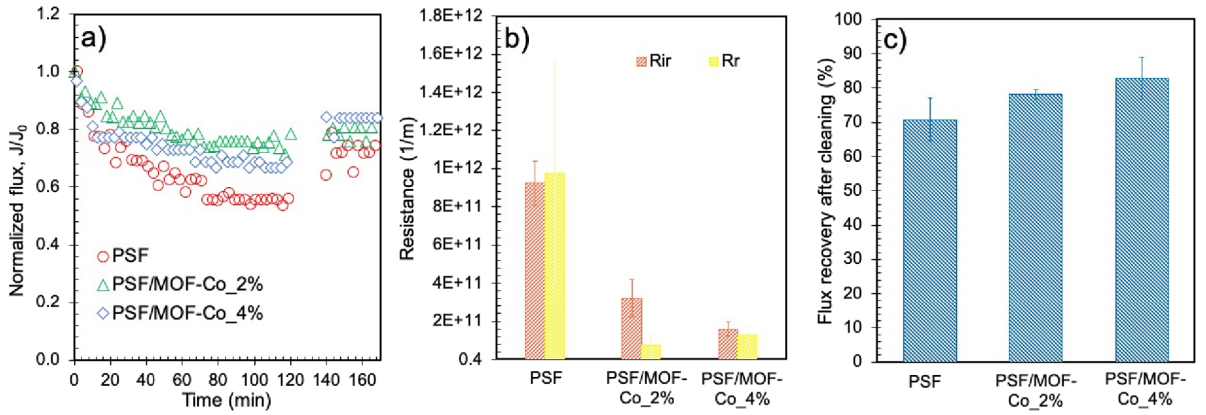

Figure 10. (a) Comparison of the membrane flux decrease in the dead-end filtration system during organic fouling experiments and after cleaning the membrane with PSF, PSF/MOF-Co_2%, and PSF/MOF-Co_4%. Total ionic strength = 10 mM, pH 8, J_0 = 108 ± 2 L/m^2-h. The organic foulant used is 20 mg/L NOM. (b) Reversible and irreversible fouling resistances during NOM solution filtration by different membranes. (c) Flux recovery after cleaning (%) of fouled PSF and MOF-Co/PSF membranes. All experiments were run in duplicates.

stability of the MOF-Co-modified membranes as well as the MOF-Co itself in long-term operation must be investigated to determine these membranes' potential for practical applications.

■ ASSOCIATED CONTENT

Supporting Information

The Supporting Information is available free of charge at https://pubs.acs.org/doi/10.1021/acsapm.2c00132.

Schematic of the bench scale ultrafiltration system (PDF)

■ AUTHOR INFORMATION

Corresponding Authors

Alejandro Zepeda − *Facultad de Ingeniería Química, Universidad Autónoma de Yucatán, Campus de Ingenierías y Ciencias Exactas, 97203 Mérida, YUC, México*; Email: zepeda74@yahoo.com, alejandro.zepeda@correo.uady.mx

Qilin Li − *Department of Civil and Environmental Engineering and Department of Chemical and Biomolecular Engineering, Rice University, Houston, Texas 77005, United States; Nanosystems Engineering Research Center for Nanotechnology Enabled Water Treatment, Houston, Texas 77005, United States; Department of Materials Science and Nanoengineering, Rice University, Houston, Texas 77005, United States;* orcid.org/0000-0001-5756-3873; Email: ql4216@rice.edu

Authors

Eva Gil − *Department of Civil and Environmental Engineering, Rice University, Houston, Texas 77005, United States; Facultad de Ingeniería Química, Universidad Autónoma de Yucatán, Campus de Ingenierías y Ciencias Exactas, 97203 Mérida, YUC, México;* orcid.org/0000-0001-7337-1636

Xiaochuan Huang − *Department of Civil and Environmental Engineering, Rice University, Houston, Texas 77005, United States; Nanosystems Engineering Research Center for Nanotechnology Enabled Water Treatment, Houston, Texas 77005, United States*

Kuichang Zuo − *Department of Civil and Environmental Engineering, Rice University, Houston, Texas 77005, United States; Nanosystems Engineering Research Center for Nanotechnology Enabled Water Treatment, Houston, Texas 77005, United States*

Jun Kim − *Department of Civil and Environmental Engineering, Rice University, Houston, Texas 77005, United States; Nanosystems Engineering Research Center for Nanotechnology Enabled Water Treatment, Houston, Texas 77005, United States; Access Business Group, Ada, Michigan 49355, United States*

Susana Rincón − *Tecnológico Nacional de Mexico/I.T. Merida, 97118 Mérida, YUC, México*

José María Rivera − *Facultad de Ciencias Químicas, Universidad Veracruzana, 94340 Orizaba, VER, México*

Kiarash Ranjbari − *Nanosystems Engineering Research Center for Nanotechnology Enabled Water Treatment, Houston, Texas 77005, United States; School of Sustainable Engineering and the Built Environment, Arizona State University, Tempe, Arizona 85281, United States*

François Perreault − *Nanosystems Engineering Research Center for Nanotechnology Enabled Water Treatment, Houston, Texas 77005, United States; School of Sustainable Engineering and the Built Environment, Arizona State University, Tempe, Arizona 85281, United States;* orcid.org/0000-0002-4756-8205

Pedro Alvarez − *Department of Civil and Environmental Engineering and Department of Chemical and Biomolecular Engineering, Rice University, Houston, Texas 77005, United States; Nanosystems Engineering Research Center for Nanotechnology Enabled Water Treatment, Houston, Texas 77005, United States; Department of Materials Science and Nanoengineering, Rice University, Houston, Texas 77005, United States;* orcid.org/0000-0002-6725-7199

Complete contact information is available at: https://pubs.acs.org/10.1021/acsapm.2c00132

Author Contributions

The manuscript was written through contributions of all authors. All authors have given approval to the final version of the manuscript.

Notes

The authors declare no competing financial interest.

https://doi.org/10.1021/acsapm.2c00132
ACS Appl. Polym. Mater. 2022, 4, 3532−3542

■ ACKNOWLEDGMENTS

The authors acknowledge the partial support by the CONACyT scholarship (CVU: 665318), CONACyT project no. 3303, and the NSF Nanosystems Engineering Research Center for Nanotechnology-Enabled Water Treatment (EEC-1449500).

■ ABBREVIATIONS

MOFs, metal−organic frameworks; MOF-Co, MOF Co_2(btec)(bipy)$(DMF)_2$; PSF, polysulfone; UF, ultrafiltration; NOM, natural organic matter; MWCNTs, multiwalled carbon nanotubes; PES, polyethersulfone; MMM, mixed matrix membrane; NF, nanofiltration; ZIF-L, zeolitic imidazolate framework; BSA, bovine serum albumin; TA, tannic acid; hZIF-8, hollow zeolitic imidazolate framework-8; PANCMA, poly(acrylonitrile-*co*-maleic acid); $(Co(NO_3)2$, cobalt nitrate hexahydrate; H_4BTEC, 1,2,4,5-benzenetetracarboxylic acid; DMF, *N*,*N*-dimethylformamide; PVP, poly(vinyl pyrrolidone); NMP, *N*-methyl-2-pyrrolidone; SDS, sodium dodecyl sulfate; PEG, polyethylene glycol; NaOH, sodium hydroxide; HCl, hydrochloric acid; $CaCl_2$, calcium chloride; NaCl, sodium chloride; ATR-FTIR, attenuated total reflectance-Fourier transform infrared spectroscopy; XRD, X-ray powder diffraction; TGA-DTG, thermal gravimetric analysis-differential thermogravimetry; FESEM, field emission scanning electron microscopy; BET, Brunauer−Emmett−Teller; SEM, scanning electron microscopy; EDS, energy-dispersive spectroscopy; AFM, atomic force microscopy; ε, overall porosity; W_w, weight of the wet membranes; W_d, weight of the dry membranes; A, membrane area; d_w, density of water; l, membrane thickness determined from the cross-sectional SEM images; KCl, potassium chloride; $KHCO_3$, potassium hydrogen carbonate; KOH, potassium hydroxide; L_p, membrane water permeability; J_w, clean water flux; ΔP, applied pressure; TOC, total organic carbon; R, rejection; C_p, PEG concentrations in the permeate solutions; C_f, PEG concentrations in the feed solutions; J_{BF}, initial clean water flux; J_{AF}, permeate flux; R_t, total hydraulic resistance; R_m, intrinsic membrane resistance; R_r, resistance of the reversible fouling layer; R_{ir}, resistance of the irreversible fouling layer; J_F, flux at the end of the fouling stage; TMP, transmembrane pressure; μ, water viscosity; FR, flux recovery; S, sulfur; Co, cobalt; R_a, arithmetic mean roughness; GO, graphene oxide; MWCO, molecular weight cutoff; MW, molecular weight; J/J_0, normalized flux

■ REFERENCES

(1) Bakker, A.; Klein-Nulend, J.; Burger, E. Shear stress inhibits while disuse promotes osteocyte apoptosis. *Biochem. Biophys. Res. Commun.* **2004**, *320*, 1163−1168.
(2) Leos, J. Z.; Zydney, A. L. *Microfiltration and Ultrafiltration*; Routledge, 2017. DOI: 10.1201/9780203747223.
(3) Reddy, A. V. R.; Patel, H. R. Chemically treated polyethersulfone/polyacrylonitrile blend ultrafiltration membranes for better fouling resistance. *Desalination* **2008**, *221*, 318−323.
(4) Susanto, H.; Ulbricht, M. Characteristics, performance and stability of polyethersulfone ultrafiltration membranes prepared by phase separation method using different macromolecular additives. *J. Membr. Sci.* **2009**, *327*, 125−135.
(5) Yurekli, Y.; Yildirim, M.; Aydin, L.; Savran, M. Filtration and removal performances of membrane adsorbers. *J. Hazard. Mater.* **2017**, *332*, 33−41.
(6) Celik, E.; Park, H.; Choi, H.; Choi, H. Carbon nanotube blended polyethersulfone membranes for fouling control in water treatment. *Water Res.* **2011**, *45*, 274−282.
(7) Zodrow, K.; Brunet, L.; Mahendra, S.; Li, D.; Zhang, A.; Li, Q.; Alvarez, P. J. J. Polysulfone ultrafiltration membranes impregnated with silver nanoparticles show improved biofouling resistance and virus removal. *Water Res.* **2009**, *43*, 715−723.
(8) Yu, W.; Brown, M.; Graham, N. J. D. Prevention of PVDF ultrafiltration membrane fouling by coating MnO2 nanoparticles with ozonation. *Sci. Rep.* **2016**, *6*, 30144.
(9) Chung, T. S.; Jiang, L. Y.; Li, Y.; Kulprathipanja, S. Mixed matrix membranes (MMMs) comprising organic polymers with dispersed inorganic fillers for gas separation. *Prog. Polym. Sci.* **2007**, *32*, 483−507.
(10) Moore, T. T.; Mahajan, R.; Vu, D. Q.; Koros, W. J. Hybrid Membrane Materials Comprising Organic Polymers with Rigid Dispersed Phases. *AIChE J.* **2004**, *50*, 311−321.
(11) Katoch, A.; Goyal, N.; Gautam, S. Applications and advances in coordination cages: Metal-Organic Frameworks. *Vacuum* **2019**, *167*, 287−300.
(12) Zhu, L.; Yu, H.; Zhang, H.; Shen, J.; Xue, L.; Gao, C.; Van Der Bruggen, B. Mixed matrix membranes containing MIL-53(Al) for potential application in organic solvent nanofiltration. *RSC Adv.* **2015**, *5*, 73068−73076.
(13) Low, Z. X.; Razmjou, A.; Wang, K.; Gray, S.; Duke, M.; Wang, H. Effect of addition of two-dimensional ZIF-L nanoflakes on the properties of polyethersulfone ultrafiltration membrane. *J. Membr. Sci.* **2014**, *460*, 9−17.
(14) Sun, H.; Tang, B.; Wu, P. Hydrophilic hollow zeolitic imidazolate framework-8 modified ultrafiltration membranes with significantly enhanced water separation properties. *J. Membr. Sci.* **2018**, *551*, 283−293.
(15) Prince, J. A.; Bhuvana, S.; Anbharasi, V.; Ayyanar, N.; Boodhoo, K. V. K.; Singh, G. Self-cleaning Metal Organic Framework (MOF) based ultra filtration membranes - A solution to bio-fouling in membrane separation processes. *Sci. Rep.* **2015**, *4*, 1−9.
(16) Song, P.; Liu, B.; Li, Y.; Yang, J.; Wang, Z.; Li, X. Two pillared-layer metal-organic frameworks constructed with Co(ii), 1,2,4,5-benzenetetracarboxylate, and 4,4′-bipyridine: Syntheses, crystal structures, and gas adsorption properties. *CrystEngComm* **2012**, *14*, 2296−2301.
(17) He, J.; Song, Y.; Chen, J. P. Development of a novel biochar/PSF mixed matrix membrane and study of key parameters in treatment of copper and lead contaminated water. *Chemosphere* **2017**, *186*, 1033−1045.
(18) Mohammadnezhad, F.; Feyzi, M.; Zinadini, S. A novel Ce-MOF/PES mixed matrix membrane; synthesis, characterization and antifouling evaluation. *J. Ind. Eng. Chem.* **2019**, *71*, 99−111.
(19) Inurria, A.; Cay-Durgun, P.; Rice, D.; Zhang, H.; Seo, D. K.; Lind, M. L.; Perreault, F. Polyamide thin-film nanocomposite membranes with graphene oxide nanosheets: Balancing membrane performance and fouling propensity. *Desalination* **2019**, *451*, 139−147.
(20) Yu, C.; Wu, J.; Contreras, A. E.; Li, Q. Control of nanofiltration membrane biofouling by Pseudomonas aeruginosa using d-tyrosine. *J. Membr. Sci.* **2012**, *423-424*, 487−494.
(21) Al-Rashdi, B. A. M.; Johnson, D. J.; Hilal, N. Removal of heavy metal ions by nanofiltration. *Desalination* **2013**, *315*, 2−17.
(22) Li, Q.; Elimelech, M. Synergistic effects in combined fouling of a loose nanofiltration membrane by colloidal materials and natural organic matter. *J. Membr. Sci.* **2006**, *278*, 72−82.
(23) Costa, A. R.; de Pinho, M. N.; Elimelech, M. Mechanisms of colloidal natural organic matter fouling in ultrafiltration. *J. Membr. Sci.* **2006**, *281*, 716−725.
(24) He, J.; Lu, X.; Yu, J.; Wang, L.; Song, Y. Hierarchical Co(OH)2 nanostructures/glassy carbon electrode derived from Co(BTC) metal−organic frameworks for glucose sensing. *J. Nanopart. Res.* **2016**, *18*, 184.
(25) Zuo, K.; Huang, X.; Liu, X.; Gil Garcia, E. M.; Kim, J.; Jain, A.; Chen, L.; Liang, P.; Zepeda, A.; Verduzco, R.; Lou, J.; Li, Q. A Hybrid Metal-Organic Framework-Reduced Graphene Oxide Nanomaterial

for Selective Removal of Chromate from Water in an Electrochemical Process. *Environ. Sci. Technol.* **2020**, *54*, 13322−13332.
(26) Abdullah, N.; Gohari, R. J.; Yusof, N.; Ismail, A. F.; Juhana, J.; Lau, W. J.; Matsuura, T. Polysulfone/hydrous ferric oxide ultrafiltration mixed matrix membrane: Preparation, characterization and its adsorptive removal of lead (II) from aqueous solution. *Chem. Eng. J.* **2016**, *289*, 28−37.
(27) Delavar, M.; Bakeri, G.; Hosseini, M. Fabrication of polycarbonate mixed matrix membranes containing hydrous manganese oxide and alumina nanoparticles for heavy metal decontamination: Characterization and comparative study. *Chem. Eng. Res. Des.* **2017**, *120*, 240−253.
(28) Ren, Y.; Li, T.; Zhang, W.; Wang, S.; Shi, M.; Shan, C.; Zhang, W.; Guan, X.; Lv, L.; Hua, M.; Pan, B. MIL-PVDF blend ultrafiltration membranes with ultrahigh MOF loading for simultaneous adsorption and catalytic oxidation of methylene blue. *J. Hazard. Mater.* **2019**, 312−321.
(29) Yang, S.; Zou, Q.; Wang, T.; Zhang, L. Effects of GO and MOF@GO on the permeation and antifouling properties of cellulose acetate ultrafiltration membrane. *J. Membr. Sci.* **2019**, *569*, 48−59.
(30) Ma, J.; Guo, X.; Ying, Y.; Liu, D.; Zhong, C. Composite ultrafiltration membrane tailored by MOF@GO with highly improved water purification performance. *Chem. Eng. J.* **2017**, *313*, 890−898.
(31) Sun, H.; Tang, B.; Wu, P. Development of Hybrid Ultrafiltration Membranes with Improved Water Separation Properties Using Modified Superhydrophilic Metal-Organic Framework Nanoparticles. *ACS Appl. Mater. Interfaces* **2017**, *9*, 21473−21484.
(32) Lee, J. Y.; Tang, C. Y.; Huo, F. Fabrication of porous matrix membrane (PMM) using metal-organic framework as green template for water treatment. *Sci. Rep.* **2014**, *4*, 1−5.
(33) Sotto, A.; Orcajo, G.; Arsuaga, J. M.; Calleja, G.; Landaburu-Aguirre, J. Preparation and characterization of MOF-PES ultrafiltration membranes. *J. Appl. Polym. Sci.* **2015**, *132*, 1−9.
(34) Ahmad, N.; Samavati, A.; Abdul, N.; Nordin, H.; Ismail, A. F.; Ahmad, N.; Nik, N. Enhanced performance and antibacterial properties of amine-functionalized ZIF-8-decorated GO for ultrafiltration membrane. *Sep. Purif. Technol.* **2020**, *239*, 116554.
(35) Feng, H.; Liu, J.; Mu, Y.; Lu, N.; Zhang, S.; Zhang, M.; Luan, J.; Wang, G. Hybrid ultrafiltration membranes based on PES and MOFs @ carbon quantum dots for improving anti-fouling performance. *Sep. Purif. Technol.* **2021**, *266*, 118586.
(36) Rana, D.; Matsuura, T. Surface Modifications for Antifouling Membranes. *Chem. Rev.* **2010**, *110*, 2448−2471.

https://doi.org/10.1021/acsapm.2c00132
ACS Appl. Polym. Mater. 2022, 4, 3532−3542